Acta Crystallographica Section D
Biological Crystallography
ISSN 0907-4449

Nickel binding to NikA: an additional binding site reconciles spectroscopy, calorimetry and crystallography

Christine Addy,[a]‡ Masato Ohara,[a]‡ Fumihiro Kawai,[a] Akinori Kidera,[a] Mitsunori Ikeguchi,[a] Sotaro Fuchigami,[a] Masanori Osawa,[b,c] Ichio Shimada,[b,c] Sam-Yong Park,[a] Jeremy R. H. Tame[a] and Jonathan G. Heddle[a,d]*

[a]Graduate School of Integrated Science, Yokohama City University, Tsurumi, Suehiro 1-7-29, Yokohama 230-0045, Japan, [b]Department of Physical Chemistry, Graduate School of Pharmaceutical Sciences, The University of Tokyo, Tokyo 113-0033, Japan, [c]Biological Information Research Center, BIRC, National Institute of Advanced Industrial Science and Technology, AIST, Aomi Koto-ku, Tokyo 135-0064, Japan, and [d]Graduate School of Materials Science, Nara Institute of Science and Technology, 8916-5 Takayama, Ikoma, Nara 630-0192, Japan

‡ These authors contributed equally to this work.

Correspondence e-mail: jgh4@tsurumi.yokohama-cu.ac.jp

Received 15 August 2006
Accepted 15 November 2006

PDB Reference: mutant NikA, 2noo, r2noosf.

Intracellular nickel is required by *Escherichia coli* as a cofactor for a number of enzymes and is necessary for anaerobic respiration. However, high concentrations of nickel are toxic, so both import and export systems have evolved to control the cellular level of the metal. The *nik* operon in *E. coli* encodes a nickel-uptake system that includes the periplasmic nickel-binding protein NikA. The crystal structures of wild-type NikA both bound to nickel and in the apo form have been solved previously. The liganded structure appeared to show an unusual interaction between the nickel and the protein in which no direct bonds are formed. The highly unusual nickel coordination suggested by the crystal structure contrasted strongly with earlier X-ray spectroscopic studies. The known nickel-binding site has been probed by extensive mutagenesis and isothermal titration calorimetry and it has been found that even large numbers of disruptive mutations appear to have little effect on the nickel affinity. The crystal structure of a binding-site mutant with nickel bound has been solved and it is found that nickel is bound to two histidine residues at a position distant from the previously characterized binding site. This novel site immediately resolves the conflict between the crystal structures and other biophysical analyses. The physiological relevance of the two binding sites is discussed.

1. Introduction

Nickel is a much rarer element than iron, its close neighbour in the periodic table, and plays a much smaller role in biology. It is nevertheless biologically important and several enzymes from *Escherichia coli* are known to be dependent on it for catalytic activity. The most medically interesting of these is urease (EC 3.5.1.5), an enzyme which is responsible for catalyzing the hydrolysis of urea into ammonia and carbamate (Mobley & Hausinger, 1989) and which is required for *Heliocobacter pylori* to withstand acid conditions and colonize the stomach (Eaton *et al.*, 1991). Nickel is transported to the active site of urease by UreE (Colpas & Hausinger, 2000; Lee *et al.*, 1993; Remaut *et al.*, 2001).

In 1993, Mandrand-Berthelot and coworkers showed that nickel is taken up by a periplasmic binding-protein-dependent system involving a soluble nickel-binding protein and an ATP-driven membrane complex encoded by the *nik* operon (Navarro *et al.*, 1993). *nikA* encodes the 502-residue periplasmic binding protein and *nikBCDE* encodes the integral membrane proteins and accompanying ATP-driven subunits.

© 2007 International Union of Crystallography
Printed in Denmark – all rights reserved

Our studies of nickel binding to NikA by isothermal titration calorimetry (ITC) showed the affinity to be unexpectedly weak, with a K_d of about 10 μM, which is one or two orders of magnitude higher than the reported K_d values for other periplasmic binding proteins. Two previous papers had reported very different K_d values for NikA. One used a spectroscopic assay involving a reporter molecule and the other used fluorimetry to observe the ligation of NikA. The first method gave a K_d value that was very similar to ours (Salins *et al.*, 2002), but the second suggested a K_d of 0.1 μM (de Pina *et al.*, 1995). We were unable to reproduce this result from fluorimetry, but the ITC data were highly reproducible and gave a good fit to a stoichiometry of one nickel ion per protein molecule, as expected.

NikA from *E. coli* was originally crystallized in 1994 by Fontecilla-Camps and coworkers (Charon *et al.*, 1994). We solved the crystal structure of the apo and nickel-bound forms several years ago (Heddle *et al.*, 2003; PDB codes 1uiu and 1uiv, respectively), showing NikA to be very similar in structure to the oligopeptide-binding protein OppA (Tame *et al.*, 1994) and the dipeptide-binding protein DppA (Dunten & Mowbray, 1995; Nickitenko *et al.*, 1995). These peptide-binding proteins have two rigid lobes separated by a flexible hinge, with the binding site lying between them. The unliganded proteins have an open structure and ligands are bound by the two lobes closing over the ligand and removing it entirely from bulk solvent. We found that with no added nickel, the apo form of the protein crystallizes with the hinge open in a manner exactly analogous to OppA and DppA. In the presence of only a twofold molar excess of nickel, the protein reproducibly gave the same unliganded crystals.

Substantial concentrations of nickel (approximately 2.5 mM) were required to crystallize the NikA–nickel complex. Unexpectedly, this showed the hinge to have closed but the nickel ion to still be exposed to the solvent. Both the liganded and apo structures were refined to high resolution (1.95 and 1.85 Å, respectively), allowing a mutation at the protein surface to immediately be identified from the electron density. Two copies of the molecule were found in each structure and comparison shows that the lobes of the protein are rigid and the hinge motion is accurately modelled by a pure rotation (rather than a screw motion) of one about the other. A metal ion could clearly be identified in the electron-density map by a single strong (>10σ) peak found at an identical position in each protein molecule in the asymmetric unit.

The nickel-binding site in the crystal structure proved to be completely unexpected. In the closed model, the electron-density map shows very strong peaks indicating the metal position, but there are no direct bonds to the protein itself and the density around the metal ion was tentatively identified as a coordination shell of water, although the bonds are unusually long at over 2.5 Å. Moreover, the only residue hydrogen-bonding to this shell of water molecules is an arginine. The only bonds driving the association between NikA and nickel ions therefore appeared to be cation–π interactions with the two tryptophan residues at the binding site. The nickel-binding site in NikA appeared unprecedented, to say the least. However, the quality of the electron-density maps and comparison with the apo form showed that the structure is substantially correct. This is further supported by the very close similarity of the protein structure to those of OppA and DppA, as well as a nearly complete set of NMR assignments for the NikA backbone which give independent confirmation of the secondary structure (Rajesh *et al.*, 2005).

Recently, an additional crystal structure of *E. coli* NikA was presented by Cherrier *et al.* (2005). This group expressed the full-length gene and then purified the mature protein (missing the signal peptide) from the periplasm. The polypeptide is identical to the NikA protein we express in the cytoplasm. This structure (PDB code 1zlq) is a different crystal form to ours and refined to 1.8 Å. This model is in the closed form and clearly has more than a simple metal ion in the binding site. By careful modelling, it was shown that the metal is chelated by EDTA, which was present in the buffers used throughout protein purification. By collecting anomalous diffraction data and directly measuring the X-ray fluorescence of the crystal, it was shown that the metal ion held by the EDTA is iron and not nickel. Iron was not added to the protein at any stage of the purification. Cherrier and coworkers suggested that iron–

Table 1
Data-collection and refinement statistics.

Values in parentheses are for the outer resolution shell (1.71–1.65 Å).

Space group	$P2_12_12_1$
Wavelength (Å)	1.0
Unit-cell parameters (Å)	a = 43.77, b = 92.24, c = 116.38
Resolution range (Å)	50–1.65
Reflections measured	269802
Unique reflections	54989
Completeness	95.9 (75.5)
R_{merge}†	5.4 (20.5)
Multiplicity	4.9
$\langle I/\sigma(I)\rangle$	8.5 (1.3)
Refinement resolution (Å)	20–1.65
σ cutoff	0
Reflections used	54867
Reflections used for R_{free}	2788
R factor‡ (%)	17.7
R_{free}‡ (%)	21.0
R.m.s.d. bond lengths (Å)	0.014
R.m.s.d. bond angles (°)	1.55
No. of water molecules	346
No. of non-H atoms (total)	4250
Average B factor (Å^2)	
Protein	16
I atoms	23
Ni atoms	23
Waters	24
Ramachandran plot	
Residues in most favourable regions (%)	90.8
Residues in additional allowed regions (%)	8.5
Residues in generously allowed regions§ (%)	0.7

† $R_{merge} = \sum I_i - \langle I\rangle|/\sum I_i$, where I_i is the intensity of observation and $\langle I\rangle$ is the mean value for that reflection. ‡ R factor = $\sum ||F_o(h)| - |F_c(h)||/\sum_h F_o(h)$, where F_o and F_c are the observed and calculated structure-factor amplitudes, respectively. The free R factor was calculated with 5% of the data excluded from the refinement. § Three residues are highlighted by *PROCHECK* as having unusual φ/ψ angles: Trp49, Lys157 and Ala400. Trp49 and Lys157 are both well defined in the electron density and adopt conformations essentially identical to those seen in PDB entry 1uiu. Pro401 seems to be partly in the *cis* conformation (and is in the *cis* conformation in 1uiu).

EDTA binds to NikA extremely tightly, preventing removal, and that our protein must also have been purified in this iron-bound form.

To investigate the metal-binding site further, we have produced a series of mutants and measured nickel binding by calorimetry. We have also solved the crystal structure of a highly mutated NikA, demonstrating that hydrated nickel ions bind to a quite different site from chelated nickel ions. This novel and probably nonphysiological binding site explains the X-ray absorbance spectroscopy and calorimetry results, which could not be reconciled with the earlier crystal structures.

2. Materials and methods

2.1. Cloning, mutagenesis, expression and purification

Cloning, expression and purification of wild-type NikA were carried out as described previously (Heddle *et al.*, 2003). In brief, the gene encoding mature NikA was cloned into pET28b (Novagen) and expressed from BL21 (DE3) cells (Invitrogen) *via* addition of IPTG. After protein expression, cells were centrifuged and the cell pellet was resuspended in 50 m*M* Tris–HCl pH 8.5, 2 m*M* EDTA, 2 m*M* DTT. Cells were lysed by sonication. Cell lysate was cleared by centrifugation and 1 *M* ammonium sulfate was added to the supernatant, which was then passed through a phenyl Sepharose column (Pharmacia) equilibrated in the same buffer. Fractions containing NikA were exchanged into 50 m*M* Tris–HCl pH 8.5, 2 m*M* EDTA, 2 m*M* DTT and then applied onto a Q-Sepharose column (Pharmacia) and eluted with an ascending NaCl gradient. Where further purification was necessary, NikA was applied onto a Hiload 26/60 Superdex 200 gel-filtration column (Pharmacia). Where EDTA-free proteins were required, the above protocol was repeated but no EDTA was added at any stage. Where DTT-free proteins were required, no DTT was added during purification. Mutant NikAs were generated using the Quikchange mutagenesis kit (Stratagene).

Nickel-free NikA was produced by purification in the presence of 20 m*M* imidazole. Protein concentrations were calculated using calculated extinction coefficients and measuring the absorbance at 280 nm.

2.2. Crystallization

Mutant NikA bound to nickel was crystallized using the hanging-drop method. Crystals were grown at 293 K using 15 mg ml^{-1} NikA in 50 m*M* Tris–HCl pH 7.5. The mother liquor contained 0.1 *M* sodium acetate pH 5.5, 30%(*w*/*v*) PEG 2000, 0.2 *M* ammonium sulfate, 5 m*M* sodium iodide and 3 m*M* nickel chloride. Crystals measuring approximately 0.2 × 0.03 mm grew as triangular prisms in space group $P2_12_12_1$ with one molecule per asymmetric unit. X-rays of wavelength 1.0 Å were used to collect diffraction data to 1.6 Å resolution at beamline BL5A at the Photon Factory, Tsukuba, Japan. Data were integrated and indexed with *HKL*-2000 and scaled with *SCALEPACK* (Otwinowski & Minor, 1997).

2.3. Refinement

Initial phases were determined using the molecular-replacement package *MOLREP* (Vagin & Teplyakov, 2000) using the coordinates of the previously solved structure of NikA (PDB code 1uiu) as a search model. The NikA model was built using *TURBO* (Roussel & Cambillau, 1989). Refinement was carried out using *REFMAC* (Murshudov *et al.*, 1999) and general data handling took place using the *CCP*4 suite (Collaborative Computational Project, Number 4, 1994). I atoms were found at four tyrosine residues and were refined using standard geometry restraints. Data-collection and refinement statistics are shown in Table 1. Structures were analyzed with *XtalView* (McRee, 1999) and *Coot* (Emsley & Cowtan, 2004). The figures were produced with *PyMOL* (DeLano, 2002). Screw motions giving the least-squares fit between structures were calculated using a C program based on the *FIT* procedure of Dr Guoguang Lu. Electron-density map images were produced using *CCP*4*mg* (Potterton *et al.*, 2004).

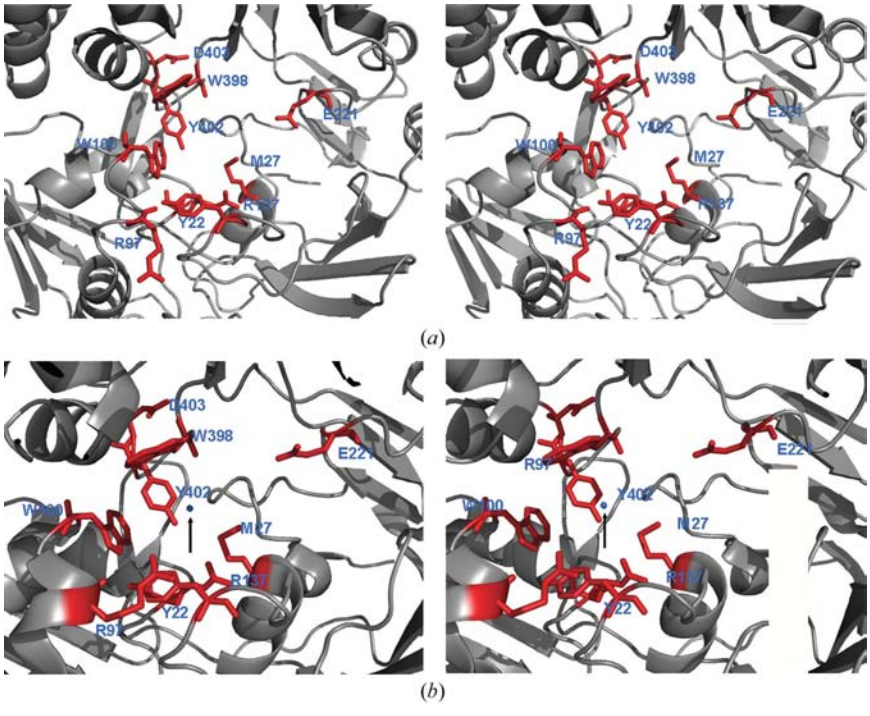

Figure 1
Stereo drawings of the nickel-binding pocket of apo NikA (*a*) and nickel-bound NikA (*b*) (PDB codes 1uiu and 1uiv, respectively). Nickel is shown as a small blue sphere (highlighted with an arrow) and surrounding waters are omitted for clarity. Residues which were mutated in this study are shown in red stick form, with the remainder of the protein shown in grey cartoon representation.

2.4. Isothermal titration calorimetry

Experiments were performed using a Microcal VP-ITC instrument. ITC buffer (50 m*M* HEPES pH 7.0, 100 m*M* NaCl) was used for both injected ligand and receptor reservoirs. NikA was generally purified using a final gel-filtration step with EDTA- and DTT-containing buffers to ensure that no free nickel remained bound to the protein. In other cases, to examine the effects of EDTA, NikA was prepared by omitting EDTA and DTT from all buffer solutions and dialyzing against 20 m*M* imidazole before the final gel-filtration step.

NikA was dialyzed into ITC buffer (50 m*M* HEPES pH 7.0, 100 m*M* NaCl) and used at a final concentration of 180–220 µ*M*. Experiments were carried out at 298 K and typically involved 18–24 injections of 1 µl $NiCl_2$ at approximately ten times the concentration of the protein. Blank runs with no protein present were used to measure the background heats of dilution. The background heats were found to be so small as to have a negligible effect on results. Each experiment was carried out two or more times and the results were analyzed with the manufacturer's software using a simple 1:1 ligand-binding site model. *N* values, the number of nickels bound per NikA, ranged from 0.33 to 1.0, probably reflecting inaccuracies in calculated extinction coefficients, the presence of a portion of misfolded protein or fitting errors.

2.5. Sequence alignment

Alignment of the amino-acid sequences of NikA proteins from 11 different bacteria and archaea were carried out using *ClustalX* (Thompson *et al.*, 1994).

2.6. Molecular-dynamics simulations

Molecular-dynamics (MD) simulations of NikA were carried out for both the unliganded and liganded forms (PDB codes 1uiu and 1uiv, respectively). The simulation systems contain 117 008 atoms (36 387 waters) and 113 951 atoms (35 363 waters) in the periodic boundary box for the unliganded and liganded forms, respectively. Some counterions were added to neutralize the system. The program *MARBLE* (Ikeguchi, 2004) and the CHARMM22 force field (Brooks *et al.*, 1983; MacKerell *et al.*, 1998) were used with the particle-mesh Ewald method (Essmann *et al.*, 1995) to evaluate the Coulombic interactions. The van der Waals parameters for the nickel ion (well depth, -0.042 kJ mol^{-1}; radius, 1.4125 Å) were determined based on *ab initio* quantum-chemical calculations using *Gaussian*03 (Gaussian, Inc.). Water and CH_x, NH_x (x = 1, 2, 3), SH and OH groups were treated as rigid bodies (Ikeguchi, 2004). After energy minimization, the system was equilibrated at constant temperature (298 K) and pressure (101.3 kPa), following production runs for 10 ns in the microcanonical ensemble. The temperature of the system was maintained at 298.1 $\pm$ 0.7 and 299.4 $\pm$ 0.7 K for the unliganded and liganded NikA, respectively.

3. Results and discussion

3.1. Isothermal titration calorimetry

We previously reported that nickel alone was able to bind to wild-type *E. coli* NikA protein with a dissociation constant of approximately 11 µ*M* (Heddle *et al.*, 2003). In order to find which residues are contributing to the binding, we constructed a series of mutants with substitutions around the known metal-

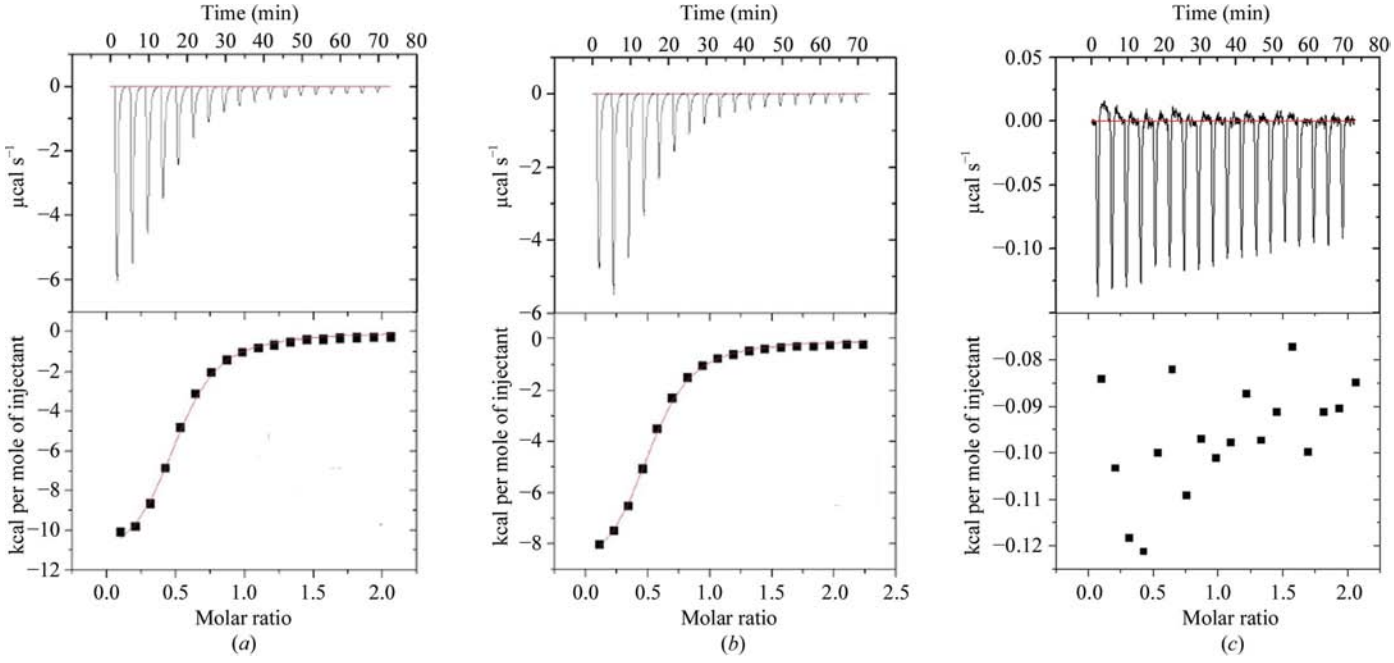

Figure 2
ITC traces of (*a*) 10 µl injections of 1.1 m*M* $NiCl_2$ into 180 µ*M* wild-type NikA and (*b*) 10 µl injections of 1.8 m*M* $NiCl_2$ into 178 µ*M* mutant (M27C) NikA and nickel. Other wild-type and mutant proteins gave similar results except for (*c*) raw data for binding of nickel to mutant H56A. 1 cal = 4.186 J.

binding site (Fig. 1). Seven mutant proteins were produced with a single residue changed: M27C, E221Q, W100H, R137E, R137A, W398A and D403N. Two more mutants were constructed: the '3-mutant' (W100H, E221Q and D403N) and the '6-mutant' (Y22A, R97A W100A, R137A, W398A and Y402A; Fig. 1*a*). When we repeated the ITC experiment using these mutants, we surprisingly found that the binding constant was unchanged (Fig. 2), implying that the nickel ion is not binding near the site identified in our previous model and by Fontecilla-Camps and coworkers (Charon *et al.*, 1994). Crystallization of the 6-mutant (see later) suggested that a new site may be present near His56, approximately 29 Å from the known metal-binding site, and a further mutation was therefore made: His56 to alanine. Titrating nickel into the H56A mutant gave no observable binding of unchelated nickel ions (Fig. 2*c*, Table 2). We repeated this experiment with nickel chelated by EDTA (Fig. 3). Firstly, we titrated nickel into EDTA to ascertain the strength of the binding under our reaction conditions. If binding is significantly tighter than nickel binding to NikA, then nickel–EDTA complex binding to the protein can be measured. We found that EDTA binds nickel extremely tightly and fitting the data gave a dissociation constant of around 14 n*M* (Fig. 3*a*). ITC is unable to measure directly and accurately an association constant greater than about 10^9 *M*, so that 14 n*M* can be used as a lower limit for tightness of binding. This is still far greater than the affinity of NikA for hydrated nickel ions. We then mixed excess EDTA with nickel to ensure all nickel was chelated and titrated this nickel–EDTA complex into a reservoir of 6-mutant NikA (Fig. 3*d*). Although this mutant was able to bind free nickel with the same affinity as the wild-type protein (Fig. 3*c*), it showed no affinity for the chelated nickel. In contrast, the wild-type protein is able to bind both chelated and free nickel, with affinities of 30 and 11 µ*M*, respectively (Figs. 3*c* and 2*a*, respectively). The H56A mutant does not bind non-chelated nickel ions, but will bind nickel–EDTA with the same affinity as the wild type (Fig. 3*b*). The binding of nickel or nickel–EDTA complexes to the wild-type NikA protein was identical regardless of whether the protein had been purified in the presence or absence of EDTA, while wild-type NikA showed no significant binding to EDTA alone (results not shown).

An obvious interpretation of these results is that there are in fact two binding sites for nickel: one between the two lobes of the protein shown in our earlier crystal structure and that of Cherrier *et al.* (2005), which binds chelated nickel, and a second, shown in our mutant crystal structure, which is able to bind hydrated nickel ions directly *via* His56.

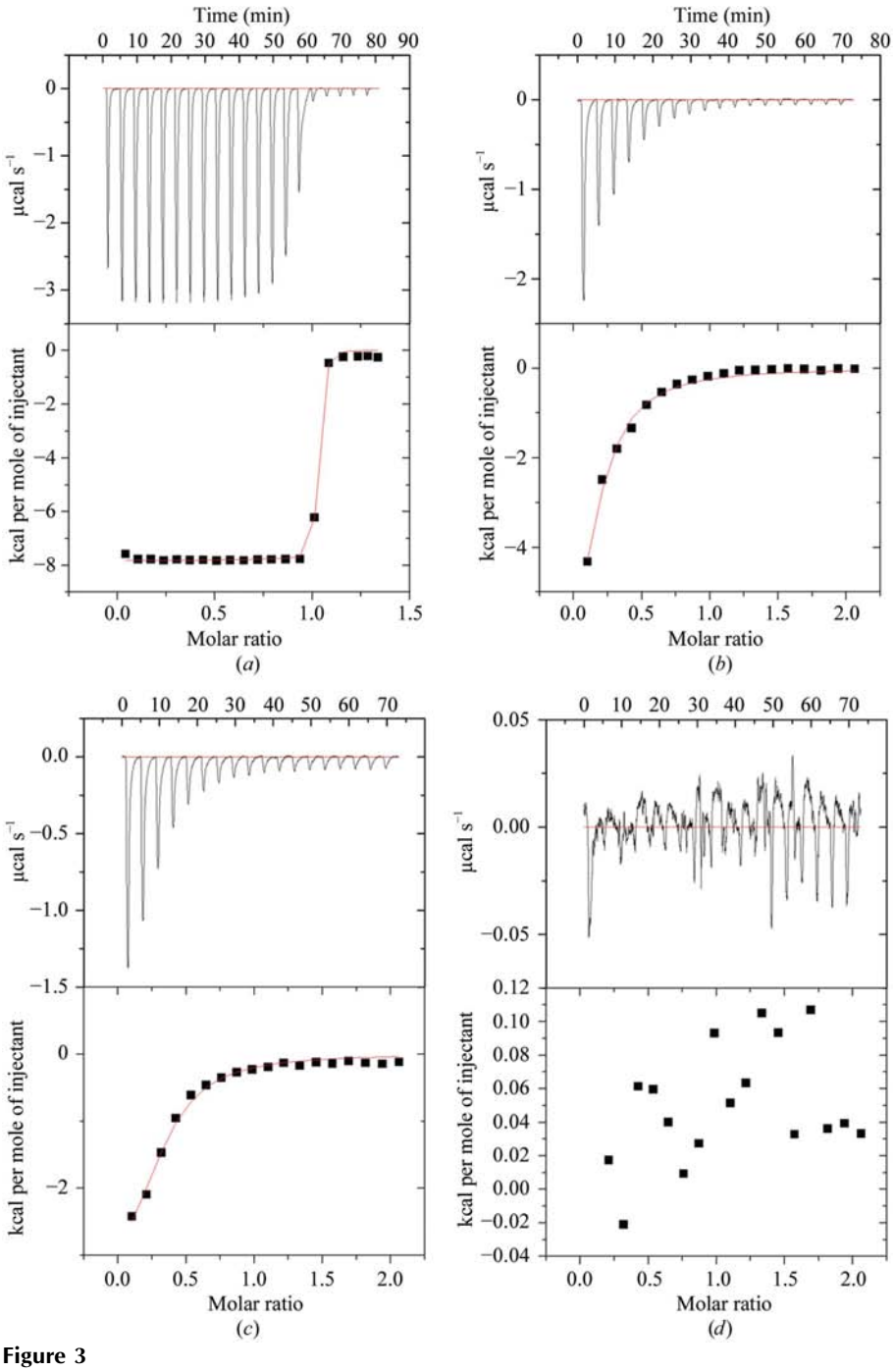

Figure 3
ITC traces of (*a*) 10 µl injections of 1.1 m*M* $NiCl_2$ into 180 µ*M* EDTA. (*b*) 10 µl injections of 5 m*M* EDTA, 1.8 m*M* $NiCl_2$ into 180 µ*M* NikA H56A. (*c*) 10 µl injections of 5 m*M* EDTA, 1.8 m*M* $NiCl_2$ into 180 µ*M* wild-type NikA. (*d*) 10 µl injections of 5 m*M* EDTA, 1.8 m*M* $NiCl_2$ into 180 µ*M* 6-mutant NikA. 1 cal = 4.186 J.

3.2. Structure determination

In conjunction with the ITC experiments, 6-mutant NikA was crystallized in the presence of nickel in an attempt to find the nickel-binding site. The protein crystallized in space group $P2_12_12_1$ as triangular prisms which diffracted to 1.65 Å. As with our earlier published structures, residues 1–3 and 501–502 were not visible in the final map, which otherwise covers the polypeptide with no breaks. The mutant NikA has an open structure highly similar to that of the wild-type apoprotein (Heddle *et al.*, 2003). It is a flattened tear-shaped protein consisting of two lobes connected by a hinge formed by two β-strands. In the mutant structure, as in the wild-type protein, no nickel is bound in the cleft between the lobes despite the protein being crystallized in the presence of a high concentration of nickel. The overall structure is shown in Fig. 4(*a*). Least-squares fitting of lobe 1 (residues 4–245 and 471–499) of the previously solved open form of NikA (PDB code 1uiu) to the same lobe in the 6-mutant (Fig. 4*b*) gave an r.m.s.d. of 1.46 Å, with the largest shifts (up to 7.3 Å) around Pro24, where there is a poorly ordered loop. Significant movements (around 3 Å) are also seen at the C-terminus. Fitting lobe 2 (residues 246–470) of both proteins gives an r.m.s.d. of 0.61 Å. Fitting one lobe and then fitting the other lobe requires a rotation of 9.0° and a translation of 1.1 Å. Fitting lobes 1 and 2 of the 6-mutant to the equivalent lobes of the previously solved closed form of the protein (PDB code 1uiv) gave r.m.s.d.s of 1.35 and 0.79 Å, respectively. Compared with 1uiv, the 6-mutant NikA structure shows an angle of 24.9° between lobes and an inter-lobe translation of 1.6 Å.

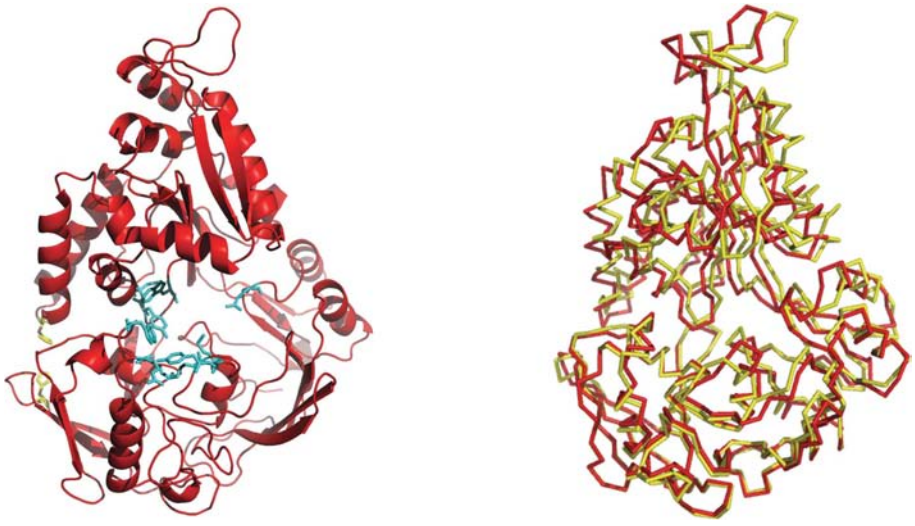

Figure 4
(*a*) Crystal structure of 6-mutant NikA. The mutated residues around the binding cleft are shown as cyan sticks. The nickel-binding histidine residues are shown as yellow sticks. (*b*) Ribbon representations of NikA (red) and 6-mutant NikA (yellow) after alignment of the C^{α} backbones of lobe 1 (residues 4–245 and 471–499) of the two proteins.

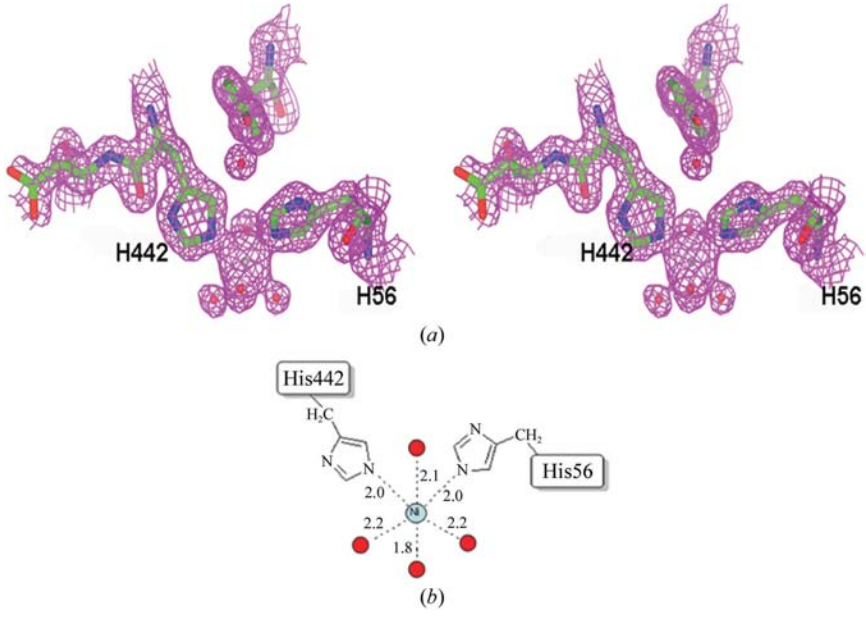

Figure 5
(*a*) Stereo drawing showing the final weighted $2F_o - F_c$ electron-density map of 6-mutant NikA at a contour level of 1.3σ covering the nickel-binding site. The nickel ion (grey) is shown bound to His56 and His442 and four coordinating water molecules. The electron density of the closest water is partially merged with that of the nickel. The Ni atom has a temperature factor of about 23 $Å^2$ and is refined with full occupancy. (*b*) Schematic diagram showing the interactions between bound nickel ions and NikA. The distances between the nickel, water molecules and the coordinating N atoms of the two histidine residues are shown in angstroms.

The protein was crystallized in the presence of sodium iodide, which we found was an aid to crystallization. Iodine was clearly visible in the structure, bound to Tyr271, Tyr284, Tyr300 and Tyr382. The first two of these tyrosines have a single I atom bound to $C^{\varepsilon 1}$ and the second two have I atoms bound to $C^{\varepsilon 1}$ and $C^{\varepsilon 2}$, although apparently without full occupancy in each case.

The most interesting feature of the mutant protein was that despite having no nickel bound in the previously defined nickel-binding pocket and an open structure, it did have a single nickel bound between two surface histidines His56 and His442 (Fig. 5). These two histidines are more than 20 Å from the main binding pocket, lying on the reverse face of the protein to the binding cleft. Comparison of the mutant structure with the previously refined unliganded NikA structure (PDB code 1uiu) shows that the structures are very similar, but with significant side-chain

Table 2
K_d values between NikA and nickel for wild-type and mutant NikAs derived from ITC.

NikA	K_d for Ni^{2+} (μM)
Wild type	10.4 ± 3.5
M27C	11.8 ± 0.5
W100H	14.0 ± 0.1
R137E	12.5 ± 7.8
R137A	6.4 ± 0.1
E221Q	15.8 ± 0.2
W398A	8.85 ± 1.3
D403N	12.5 ± 0.3
Y22A, R97A, W100A, R137A, W398A, Y402A	21.6 ± 0.27
H56A	No binding

movements around the nickel-binding site. There is a steric clash between an iodine bound to Tyr300 and the wild-type position of Tyr127. This forces Tyr127 to change rotamer, breaking a hydrogen bond between its hydroxyl group and that of Tyr451. In turn, Tyr127 presses against His442, pushing it into a suitable position to bind nickel. Addition of iodide to the crystallization trials has serendipitously revealed the new nickel-binding site. His56 lies on a hairpin loop between β-strands and the main chain has also shifted in this region in order to accommodate nickel binding. Crystallization of the wild-type protein apparently displaces nickel from this binding site. These changes in protein structure imply a significant energy cost in creating the nickel-binding site, so simulations were examined to see whether the rotamer changes are energetically reasonable in the unmodified wild-type protein.

3.3. MD simulations

In MD simulations of both liganded and unliganded NikA, the side chain Tyr127 was more mobile than expected from previous crystal structures. It occasionally changed its χ_1 angle to about -70° (see supplementary material[1]), which is close to that observed in the nickel-binding site of the mutant structure. The total residence times of this conformational state within the 10 ns simulations were 0.6 and 1.8 ns for unliganded and liganded forms, respectively. This indicates that even in the absence of nickel and iodine, NikA has a certain probability of motions forming the new nickel-binding site. Alignments of the NikA amino-acid sequences using *ClustalX* showed that the residues implicated in binding chelated nickel in the main binding cleft are mainly conserved (Fig. 6). However, the nickel-binding histidine residues His56 and His442 were not at all well conserved, being present in only two of the 11 sequences. It therefore seems unlikely that His56 and His442 represent physiologically important nickel-binding residues.

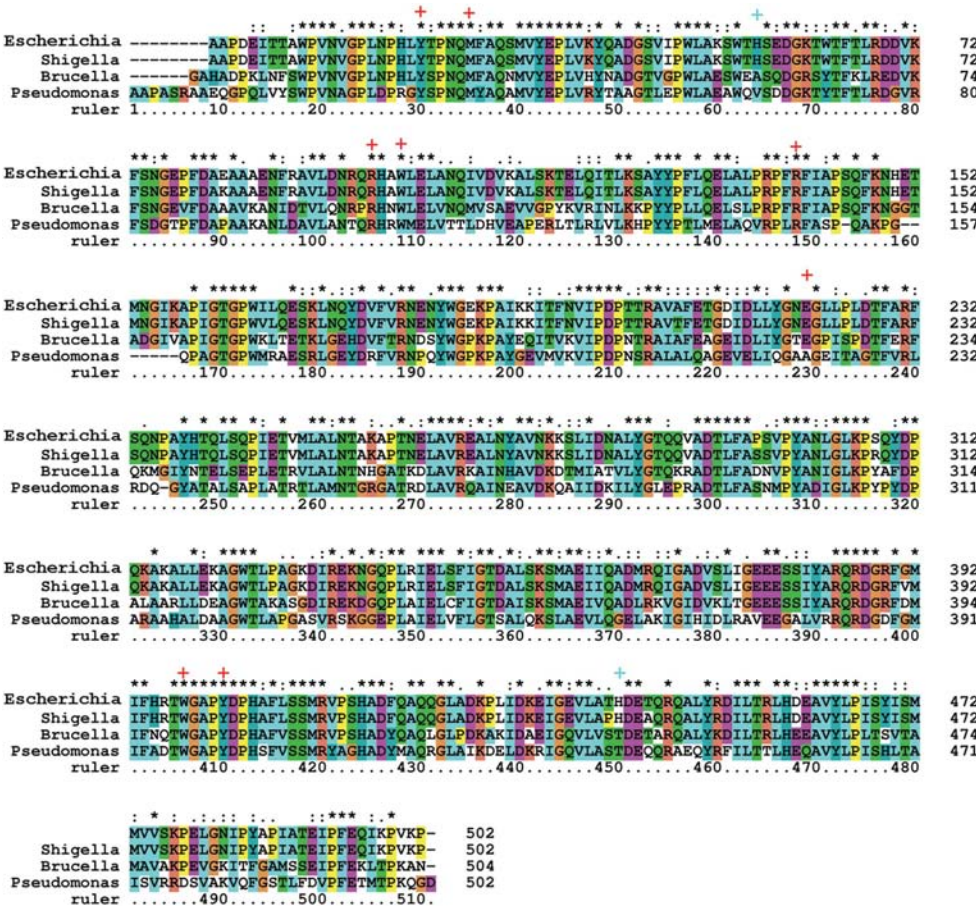

Figure 6
ClustalX alignment of known or putative NikA amino-acid sequences from *E. coli*, *Shigella dysenteria*, *Brucella suis* and *Pseudomonas putida*. Asterisks indicate completely conserved residues, colons imdicate highly similar residues and dots indicate weakly similar residues. Red crosses show the positions of the residues of NikA in the binding cleft which were mutated. These residues are largely conserved. Cyan crosses show the positions of His54 and His442, which are not conserved.

4. Conclusion

The crystal structures of NikA solved to date (Cherrier *et al.*, 2005; Heddle *et al.*, 2003) have given a contradictory picture of nickel binding to NikA. Nickel was found at first to bind to the large cleft between the two lobes of the protein (Heddle *et al.*, 2003), exactly where a periplasmic binding protein is expected to bind its ligand (Dwyer & Hellinga, 2004). However, nickel appeared to be able to bind both alone and when chelated by EDTA. Other similar binding

[1] Supplementary material has been deposited in the IUCr electronic archive (Reference: BE5071). Services for accessing this material are described at the back of the journal.

proteins such as FhuD (Clarke *et al.*, 2000) require a chelator to present the metal to the binding site, but EDTA is unlikely to be a physiological chelator as it does not occur in nature.

A recent paper describing another crystal form of NikA (Cherrier *et al.*, 2005) pointed out the highly unusual nickel-binding site reported by us previously and contrasts this with an earlier XAFS analysis, which suggested oxygen and nitrogen coordination with a bond length of 2.06 Å. This study finds that Fe^{III}-EDTA$(H_2O)^-$ binds to NikA with very high affinity and cannot be removed, so that unliganded protein cannot be produced once it has bound EDTA. As no iron was added, the presence of this metal implies a very high affinity of the iron–EDTA complex for NikA. The protein-purification protocol we used in our studies involved a final gel-filtration step with EDTA-containing buffer. It could therefore be concluded that the protein we produced must also have EDTA tightly bound and the metal ion must be iron and not nickel. This hypothesis would then explain our inability to reproduce the reported fluorescence-monitored titration with Ni^{2+} ions (de Pina *et al.*, 1995) and the low affinity we observe by ITC (Heddle *et al.*, 2003). If so, it would mean that our previous report is erroneous in two major respects: (i) that the protein carries an Fe^{3+} ion, not Ni^{2+}, and (ii) that the metal is coordinated to EDTA, a molecule so tightly held by the protein that it cannot be removed by competition with nickel ions or ferrichrome or by dilution.

At first, we checked our own previously solved structure to see if the nickel present was in fact bound to EDTA. We found that EDTA can indeed be modelled into our structure although not unambiguously. We have furthermore shown, through the crystallization of apo-NikA and our extensive ITC experiments, that the wild-type protein purified by our methods is not irreversibly liganded with Fe–EDTA as has been suggested (Cherrier *et al.*, 2005). The metal ion present in the liganded structure presented earlier by us can therefore only be the added nickel. This is confirmed by XAFS analysis of NikA prepared by us, which shows no substantial amounts of any metal such as iron or nickel to be present (M. Maroney, personal communication). Mass-spectroscopic analysis also shows no detectable ligand (such as EDTA) bound to the protein. Nevertheless, the ITC data presented here show unequivocally that nickel–EDTA does indeed bind to the site we identified in our earlier paper and hydrated nickel ions do not. The tentative coordination shell suggested by us earlier is not correct and it appears that despite dialysis some residual EDTA did remain in the sample as suggested by Cherrier *et al.* (2005). It remains unclear why very high nickel concentrations were required to obtain the liganded crystal form. Nevertheless, while EDTA has a very strong affinity for nickel, the nickel–EDTA complex has a fairly weak affinity for the wild-type NikA protein ($K_d \simeq 30\ \mu M$). This is perhaps not surprising given that EDTA is unlikely to be the *in vivo* chelating molecule and further work is required to find what the natural chelator(s) is/are. The weak binding suggests that EDTA is unlikely to be highly occupied and ordered in the crystal structure (PDB code 1uiv).

We successfully crystallized the 6-mutant NikA in the presence of nickel and found that the gross structure was unchanged. This mutant NikA did not have nickel bound in the previously defined binding site, but at a distal site between two histidine residues (His56 and His442). Binding of nickel to these histidines is similar to that in more conventional nickel-binding proteins such as UreE from *Klebsiella aerogenes* (Song *et al.*, 2001) and matches very closely that expected from the XAFS studies carried out by the Maroney group prior to solution of the protein structure (Allan *et al.*, 1998; Carrington *et al.*, 2002). It is clear that the XAFS results obtained from adding unchelated nickel ions to NikA reflect the binding at this site and not the metal site found in previous NikA structures.

Mutating one of the histidines (His56) to alanine resulted in complete loss of nickel binding as measured by ITC. Alignment of NikA sequences from a number of species shows that while the residues of the binding cleft are conserved, His56 and His442 are not. This suggests that the nickel-binding site between these histidines is unlikely to be biologically relevant and the most likely model for nickel binding to NikA *in vivo* must be one in which a nickel ion is bound as a chelator complex. The affinity of FhuD for ferrichrome iron is 0.1 μM (Braun *et al.*, 1998; Mademidis *et al.*, 1997), but our own experiments suggest that NikA does not bind ferrichrome (results not shown). The true chelator remains to be found. A second function of NikA is to control the chemotactic response of *E. coli* away from nickel. Liganded NikA binds to the chemoreceptor protein Tar, triggering demethylation (Barkai & Leibler, 1997; de Pina *et al.*, 1995), and the possibility therefore remains that the surface binding site in some way affects this binding at high nickel concentration. Further studies on this interaction are under way.

We thank Professors Eleanor Dodson, Gideon Davies and Phil Evans for commenting on our electron-density maps and models of liganded NikA. JGH was funded by a JST CREST research fellowship.

References

Allan, C. B., Wu, L.-F., Gu, Z., Choudhury, S. B., Al-Mjeni, F., Sharma, M. L., Mandrand-Berthelot, M.-A. & Maroney, M. J. (1998). *Inorg. Chem.* **37**, 5952–5955.

Barkai, N. & Leibler, S. (1997). *Nature (London)*, **387**, 913–917.

Braun, V., Hantke, K. & Koster, W. (1998). *Metal Ions in Biological Systems*, edited by A. Sigel & H. Sigel, pp. 67–145. New York: Marcel Dekker.

Brooks, B. R., Bruccoleri, R. E., Olafson, B. D., States, D. J., Swaminathan, S. & Karplus, M. (1983). *J. Comput. Chem.* **4**, 187–217.

Carrington, P. E., Al-Mjeni, F., Zoroddu, M. A., Costa, M. & Maroney, M. J. (2002). *Environ. Health Perspect.* **110**, 705–708.

Charon, M. H., Wu, L. F., Piras, C., de Pina, K., Mandrand-Berthelot, M. A. & Fontecilla-Camps, J. C. (1994). *J. Mol. Biol.* **243**, 353–355.

Cherrier, M. V., Martin, L., Cavazza, C., Jacquamet, L., Lemaire, D., Gaillard, J. & Fontecilla-Camps, J. C. (2005). *J. Am. Chem. Soc.* **127**, 10075–10082.

Clarke, T. E., Ku, S. Y., Dougan, D. R., Vogel, H. J. & Tari, L. W. (2000). *Nature Struct. Biol.* **7**, 287–291.

Collaborative Computational Project, Number 4 (1994). *Acta Cryst.* D**50**, 760–763.
Colpas, G. J. & Hausinger, R. P. (2000). *J. Biol. Chem.* **275**, 10731–10737.
DeLano, W. L. (2002). *The PyMOL Molecular Visualization System.* DeLano Scientific, San Carlos, CA, USA. http://www.pymol.org.
Dunten, P. & Mowbray, S. L. (1995). *Protein Sci.* **4**, 2327–2334.
Dwyer, M. A. & Hellinga, H. W. (2004). *Curr. Opin. Struct. Biol.* **14**, 495–504.
Eaton, K. A., Brooks, C. L., Morgan, D. R. & Krakowka, S. (1991). *Infect. Immun.* **59**, 2470–2475.
Emsley, P. & Cowtan, K. (2004). *Acta Cryst.* D**60**, 2126–2132.
Essmann, U., Perera, L., Berkowitz, M. L., Darden, T., Lee, H. & Pedersen, L. G. (1995). *J. Chem. Phys.* **103**, 8577–8593.
Heddle, J., Scott, D. J., Unzai, S., Park, S.-Y. & Tame, J. R. H. (2003). *J. Biol. Chem.* **278**, 50322–50329.
Ikeguchi, M. (2004). *J. Comput. Chem.* **25**, 529–541.
Lee, M. H., Pankratz, H. S., Wang, S., Scott, R. A., Finnegan, M. G., Johnson, M. K., Ippolito, J. A., Christianson, D. W. & Hausinger, R. P. (1993). *Protein Sci.* **2**, 1042–1052.
MacKerell, A. D. Jr, Brooks, B., Brooks, C. L., Nilsson, L., Roux, B., Won, Y. & Karplus, M. (1998). In *The Encyclopedia of Computational Chemistry*, edited by P. von R. Schleyer. Chichester: John Wiley & Sons.
McRee, D. E. (1999). *J. Struct. Biol.* **125**, 156–165.
Mademidis, A., Killmann, H., Kraas, W., Flechsler, I., Jung, G. & Braun, V. (1997). *Mol. Microbiol.* **26**, 1109–1123.
Mobley, H. L. & Hausinger, R. P. (1989). *Microbiol. Rev.* **53**, 85–108.
Murshudov, G. N., Vagin, A. A., Lebedev, A., Wilson, K. S. & Dodson, E. J. (1999). *Acta Cryst.* D**55**, 247–255.
Navarro, C., Wu, L. F. & Mandrand-Berthelot, M. A. (1993). *Mol. Microbiol.* **9**, 1181–1191.
Nickitenko, A. V., Trakhanov, S. & Quiocho, F. A. (1995). *Biochemistry*, **34**, 16585–16595.
Otwinowski, Z. & Minor, W. (1997). *Methods Enzymol.* **276**, 307–326.
Pina, K. de, Navarro, C., McWalter, L., Boxer, D. H., Price, N. C., Kelly, S. M., Mandrand-Berthelot, M. A. & Wu, L. F. (1995). *Eur. J. Biochem.* **227**, 857–865.
Potterton, L., McNicholas, S., Krissinel, E., Gruber, J., Cowtan, K., Emsley, P., Murshudov, G. N., Cohen, S., Perrakis, A. & Noble, M. (2004). *Acta Cryst.* D**60**, 2288–2294.
Rajesh, S., Heddle, J. G., Kurashima-Ito, K., Nietlispach, D., Shirakawa, M., Tame, J. R. H. & Ito, Y. (2005). *J. Biol. NMR*, **32**, 177.
Remaut, H., Safarov, N., Ciurli, S. & Van Beeumen, J. (2001). *J. Biol. Chem.* **276**, 49365–49370.
Roussel, A. & Cambillau, C. (1989). *Silicon Graphics Geometry Partners Directory*, pp. 77–78. Mountain View, CA, USA: Silicon Graphics.
Salins, L. L., Goldsmith, E. S., Ensor, C. M. & Daunert, S. (2002). *Anal. Bioanal. Chem.* **372**, 174–180.
Song, H. K., Mulrooney, S. B., Huber, R. & Hausinger, R. P. (2001). *J. Biol. Chem.* **276**, 49359–49364.
Tame, J. R. H., Murshudov, G. N., Dodson, E. J., Neil, T. K., Dodson, G. G., Higgins, C. F. & Wilkinson, A. J. (1994). *Science*, **264**, 1578–1581.
Thompson, J. D., Higgins, D. G. & Gibson, T. J. (1994). *Nucleic Acids Res.* **22**, 4673–4680.
Vagin, A. & Teplyakov, A. (2000). *Acta Cryst.* D**56**, 1622–1624.